Cation Ordering, Domain Growth, and Zinc Loss in the Microwave Dielectric Oxide $Ba_3ZnTa_2O_{9-\delta}$

Mario Bieringer,[†,||] Sandra M. Moussa,[†] Liam D. Noailles,[†] Andrew Burrows,[§] Christopher J. Kiely,[†,§] Matthew J. Rosseinsky,*[,†] and Richard M. Ibberson*[,‡]

Department of Chemistry, University of Liverpool, Liverpool, L69 7ZD United Kingdom, ISIS Facility, CLRC−Rutherford Appleton Laboratory, Chilton, Didcot, Oxon., OX11 0QX United Kingdom, and Materials Science Division, Department of Engineering, University of Liverpool, L69 3BX United Kingdom

Received July 22, 2002. Revised Manuscript Received October 29, 2002

The perovskite $Ba_3ZnTa_2O_9$ (BZT) is the parent of a family of high dielectric constant, low-loss oxides currently applied in mobile telecommunications base stations. The preparation of BZT microwave dielectric resonators with optimal dielectric properties requires careful attention to thermal treatment to control the formation of domains in which the Ta and Zn cations order on the octahedral sites of the perovskite structure. In this paper we use powder X-ray and neutron diffraction together with X-ray fluorescence and electron microscopy to demonstrate the strong correlation between the size of the cation-ordered domains, the extent of the ordering within them, and their composition, particularly the ZnO content. Phase separation into two trigonal BZT phases, which differ in the extent of cation order and the size of the ordered domains, is a common feature of all the synthetic procedures. A zinc-deficient impurity phase of nominal stoichiometry $Ba_8ZnTa_6O_{24}$, involving face- as well as corner-sharing octahedra, is identified in strongly zinc-deficient samples. A mechanism in which a fully ordered BZT phase grows at the expense of a slightly Zn-deficient and partially ordered phase is proposed.

Introduction

Microwave dielectric oxides are used as resonators in mobile telecommunication base stations.[1,2] This application requires high dielectric constants ($\epsilon_r \approx 30$) and low dielectric losses ($Q = 1/\tan\delta \approx 50-70000$) in the microwave (GHz) region, as well as a temperature coefficient of the resonant frequency (τ_f) close to zero. The formation of complex oxide materials into dense ceramic resonators with these properties requires careful and demanding processing. $Ba_3ZnTa_2O_9$ (BZT) is a widely used microwave dielectric oxide, which has excellent materials properties when processed correctly but is difficult to optimize on a commercial scale. This is a significant problem due to the cost and scarcity of Ta. The atomic-scale structure of BZT depends sensitively on the processing conditions since they control the extent to which the octahedral B sites of the parent simple perovskite are occupied in an ordered manner by the Zn and Ta cations. The relaxor ferroelectrics and piezoelectrics in the $Pb(Mg_{1/3}Nb_{2/3})O_3$ family also have properties controlled by small differences in cation ordering over various length scales, and B-site cation ordering is relevant to systems under consideration as fuel-cell components,[3] making these complex cation-ordering processes in perovskites of considerable general interest.[4]

The 2:1 cation-ordered form of BZT was reported first by Jacobson et al.[5] in space group $P\bar{3}m1$. The structure comprises single layers of Zn^{2+} octahedral B-site cations alternating with double layers of Ta^{5+} cations perpendicular to the ⟨111⟩ direction of the cubic subcell. (Figure 1) This cation order develops on high-temperature annealing from a B-site disordered cubic perovskite precursor formed in an initial lower temperature calcination step. Enhanced cation ordering (which can be quantified via both (a) the spatial extent of the ordered domains and (b) the magnitude of the order parameter, defined as the extent of Zn and Ta segregation over the two octahedral sites in the cell, within the domains) was demonstrated[6] to improve the *Q*-values of pure BZT. This was suggested to be the origin of the extreme sensitivity of *Q* to processing. The extent of B-cation ordering in this study was evaluated, as has been common in this area, using the intensity of the strongest superstructure reflection in the X-ray diffraction pattern. Complete ordering was found after treatment at 1350 °C for 120 h, with coexistence of distorted trigonal

* To whom correspondence should be addressed. E-mail: m.j.rosseinsky@liv.ac.uk (M.J.R.); r.m.ibberson@rl.ac.uk (R.M.I.).
† Department of Chemistry, University of Liverpool.
‡ CLRC−Rutherford Appleton Laboratory.
§ Department of Engineering, University of Liverpool.
|| Present address: Institut Laue Langevin, 6 rue Jules Horowitz, 38042 Grenoble, France.

(1) Vanderah, T. A. *J. Res. Natl. Inst. Stand. Technol.* **1996**, *101*, 797−802.
(2) Cava, R. J. *J. Mater. Chem.* **2001**, *11*, 54−62.
(3) Norby, T. *J. Mater. Chem.* **2001**, *11*, 11−18.
(4) Davies, P. K. *Curr. Opin. Solid State Mater. Sci.* **1999**, *4*, 467−471.
(5) Jacobson, A. J.; Collins, B. M.; Fender, B. E. F. *Acta Cryst., Sect. B: Struct. Sci.* **1976**, *32*, 1083−1087.
(6) Kawashima, S.; Nishida, M.; Ueda, I.; Ouchi, H. *J. Am. Ceram. Soc.* **1983**, *66*, 421−423.

10.1021/cm020461e CCC: $25.00
Published on Web 01/04/2003

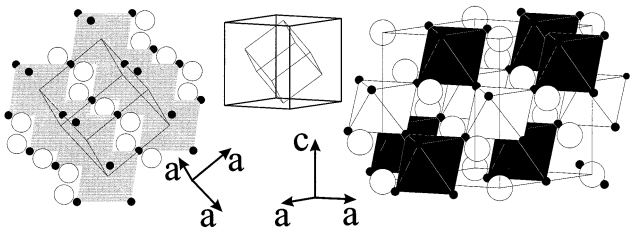

Figure 1. Illustration of the crystal structure of the perovskite subcell (left), the trigonal $P\bar{3}m1$ supercell (right), and their relation (center: the ⟨111⟩ direction of the cubic subcell is aligned with the *c*-axis of the trigonal supercell) for $Ba_3ZnTa_2O_9$. Gray octahedra represent disordered Zn/TaO_6 units, white octahedra represent ZnO_6 units, and black octahedra represent TaO_6 units. White circles denote Ba^{2+} cations.

and undistorted cubic phases being deduced qualitatively from laboratory X-ray data collected from samples annealed for shorter periods.

The processing of BZT is however complex, and materials loss as well as the development of Zn/Ta site ordering can occur during sintering and annealing, affecting both the X-ray intensities and the microwave dielectric properties. Desu and O'Bryan[7] demonstrated that ZnO loss during BZT preparation results in increased *Q*-values. The presence of additional unidentified phases on the pellet surface was reported but no detailed structural analysis of the BZT phase was carried out. The continued evolution of the *c*/*a* ratio when the superstructure intensities had saturated lead these authors to conclude that Zn loss coupled with Ba substitution at the B-site was occurring. ZnO loss from BZT ceramics enhances Q in a reversible manner.[8]

The long annealing times required for full cation order, and the corresponding high *Q* values, to be attained preclude commercial application of pure BZT. Zr doping on the B-site significantly accelerates the cation-ordering process [4,9,10] allowing very high *Q*-values to be achieved after only a few hours of annealing. The resulting cation-ordered domains are reduced in size compared with pure $Ba_3ZnTa_2O_9$, suggesting that the high losses in partially ordered BZT are due to elastic strains at the domain wall boundaries. The role of Zr is suggested to be minimizing this strain,[11] thereby removing the need to grow the volume of the ordered domains to minimize the influence of these boundaries.

No additional quantitative work on pure $Ba_3ZnTa_2O_9$ using modern diffraction techniques has been reported since the original publication in 1976. Understanding the structural consequences of ZnO loss on the composition, order parameter, and ordered domain size of BZT is a taxing problem to resolve using only single-reflection analysis of medium-resolution laboratory powder X-ray data and requires a more detailed approach. In this paper we employ simultaneous analysis of high-resolution synchrotron and neutron diffraction data together with laboratory X-ray data. This allows us to quantify the effect of processing conditions on the physical and chemical extent of B-site ordering and to identify the impurity phase competing with the formation of high *Q* BZT. The influence of ZnO loss during processing on the composition and structure of BZT is also examined, revealing a close relationship to phase separation and ordered domain growth. Previous studies have suggested that B-site order or Zn loss control the variation of *Q* in the BZT system—the present study reveals that these two phenomena are closely related to each other.

Experimental Section

Polycrystalline samples of $Ba_3ZnTa_2O_9$ were prepared from stoichiometric starting mixtures of $BaCO_3$ (Solvay), ZnO (Durham Electrox 2500), and Ta_2O_5 (H. C. Starck), according to the reaction

$$3BaCO_3 + ZnO + Ta_2O_5 \rightarrow Ba_3ZnTa_2O_9 + 3CO_2$$

Sample Synthesis for the Identification of Preparative Parameters. A set of closely related BZT samples was prepared to follow the phase formation as a function of preparation conditions. The precursors were ball-milled in distilled water overnight using magnesia-stabilized zirconia beads. The dried powders were calcined for 4 h at 1100 °C (BZT-a). The intermediate was again ball-milled and calcined for 10 h at 1300 °C (BZT-b). The doubly calcined products were pelletized, buried in identical powder, and heated for 20 h at 1425 °C inside a covered Al_2O_3 crucible (BZT-c). The pelletized, doubly calcined material, BZT-b, was heated for 2 weeks at 1150 °C in an open crucible to afford BZT-d. BZT-b was also heated as a pellet for 2 weeks at 1350 °C in an open crucible to yield BZT-e.

Annealing Studies. A second set of samples was prepared to investigate the correlation suggested between the growth of cation-ordered superstructure domains and the formation of impurity phase(s) through the possible route of ZnO loss. The starting materials were ball-milled overnight in water using magnesia-stabilized zirconia beads. The firing consisted of a calcination step at 1200 °C for 4 h. After adding 2 wt % of the organic binder poly(ethylene glycol) (PEG), the calcined products were again ball-milled in water for 14 h. The dried powders were pelletized (13-mm pellets), placed on powder of identical composition in Al_2O_3 crucibles, and covered completely with the same powder. The crucibles were then covered with flat lids to minimize materials loss during heating. The heating program consisted of 1 h at 1550 °C followed by 6 days at 1425 °C. All heating and cooling steps were carried out with 3 °C/min ramp rates. Previous workers used temperatures of 1350−1525 °C, but no experiments with initial high-temperature sintering followed directly by a lower annealing temperature have been reported. This processing yielded sample BZT-f, in both a pellet and powder form. These two samples are important for comparative purposes as they have been treated under the same thermal conditions but with different Zn concentrations due to different Zn loss kinetics from the pellet and the powder arising from the differing surface areas.

Structural Characterization. Laboratory X-ray powder diffraction data were collected in Bragg−Brentano geometry using Cu $K\alpha_1$ radiation ($\lambda = 1.54059$ Å) with a linear position-sensitive detector using a STOE Stadi-P diffractometer. High-resolution powder neutron diffraction data were collected on the time-of-flight diffractometer HRPD at the ISIS spallation neutron source, Rutherford Appleton Laboratory, UK. Synchrotron X-ray powder data ($\lambda = 1.000057$ Å) were collected in flat plate geometry on station 2.3 at the Synchrotron Radiation Source, Daresbury Laboratory, UK. The powder diffraction data were analyzed using the Rietveld refinement package GSAS.[12] Overall compositions of the products were determined using X-ray fluorescence by the London and Scandinavian Metals Company (it should be noted that these

(7) Desu, S. B.; O'Bryan, H. M. *J. Am. Ceram. Soc.* **1985**, *68*, 10546−10551.
(8) Kawashima, S. *Am. Ceram. Soc. Bull.* **1993**, *72*, 120−126.
(9) Chai, L.; Davies, P. K. *J. Am. Ceram. Soc.* **1997**, *80*, 1727−1740.
(10) Tamura, H.; Konoike, T.; Sakabe, Y.; Wakino, K. *J. Am. Ceram. Soc.* **1984**, *67*, C59−C61.
(11) Davies, P. K.; Tong, J. Z.; Negas, T. *J. Am. Ceram. Soc.* **1997**, *80*, 1727−1740.

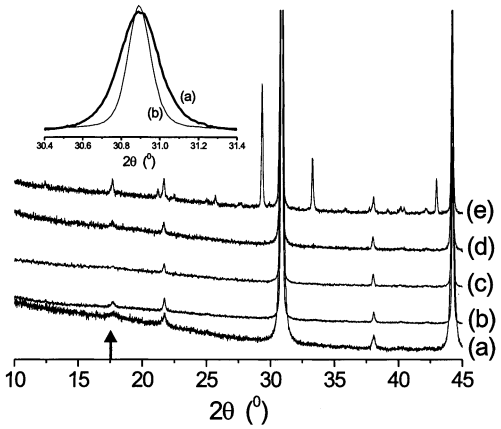

Figure 2. Laboratory X-ray data (λ = 1.54059 Å) for BZT samples a−e discussed in the text obtained at different stages of preparation. All patterns are re-normalized with respect to the peak height of the main (110/102) subcell peak at 30.9°. The arrow indicates the calculated position of the (100) superstructure peak at 17.5°. The inset shows the contrasting peak width of the main subcell peak for BZT-a and BZT-b.

analyses also demonstrated that the products were not contaminated by the milling medium).

Electron Microscopy. Samples for transmission electron microscopy analysis were prepared from the BZT-f *pellet* and *powder* samples by grinding in high-purity ethanol. A drop of the suspension was then deposited onto a holey carbon grid and the solvent was allowed to evaporate. Samples were examined in a JEOL 2000EX high-resolution electron microscope operating at 200 kV. Fourier transform (FT) analyses of the lattice fringe images obtained were carried out using Digital Micrograph.

Results

Crystallinity and Cation Ordering. Samples BZT-a−f were investigated initially using laboratory powder X-ray diffraction (Figure 2). The domain sizes, D, in Å for the samples can be estimated with the Scherrer equation

$$D = \frac{0.9\lambda}{B \cos \theta}$$

where λ is the wavelength in Å, B is the integral breadth in radians, and θ is the diffraction angle. The instrumental contribution to the fwhm for the (100) reflection is 0.11° 2θ. The calculated domain sizes based on the supercell (1 0 0) and subcell ((110) + (102)) peaks as well as an estimate of the degree of cation ordering are summarized in Table 1. In this case the normalized intensity ratio, IR, is defined as

$$\mathrm{IR} = I(100)/(I((110)+(102)) \times 0.032)$$

where I denotes the integrated intensities of the subcell and supercell reflections and 0.032:1 is the expected integrated intensity ratio of these reflections for a fully ordered phase. The (100) reflections were fitted to a Lorentzian line shape and the (110) + (102) reflections were fitted to a single pseudo-Voigt function. This analysis provides a helpful initial characterization of the materials produced but, as shown below, overly simplifies the true structural details.

Table 1. Analysis of Single Superstructure and Substructure Peaks of BZT Samples (a)−(e) and BZT-f Pellet and Powder[a]

sample	(100) fwhm (2θ = 17.7°) (deg)	D_{trig} (Å)	IR	(110) + (102) fwhm (2θ = 30.9°) (deg)
BZT-a	0.91(37)	63(39)	0.47(29)	0.249(2)
BZT-b	0.323(12)	250(14)	0.63(4)	0.143(1)
BZT-c				0.139(1)
BZT-d	0.337(26)	221(19)	0.53(5)	0.155(1)
BZT-e	0.173(11)	790(42)	0.83(6)	0.157(8)
BZT-f pellet	0.245(12)	375(11)	0.89(3)	0.138(1)
BZT-f powder	0.181(8)	696(22)	0.78(3)	0.165(2)

[a] IR is the ratio of the intensities of the supercell (100) and subcell (110 + 102) intensities as a fraction of that expected for a fully ordered phase, as discussed in the text.

It can be seen that after calcining the precursors at 1100 °C for 4 h (BZT-a) a BZT phase is formed, albeit poorly crystallized. The presence of the broad (100) superstructure reflection (2$\theta \approx$ 17.7°) for this sample indicates 2:1 ordering and the formation of small (63(39) Å) domains of the trigonal perovskite phase even at a temperature as low as 1100 °C. The inset to Figure 2 compares the broad main cubic reflection of BZT-a with the sharper peak for BZT-b, which was fired for 10 h at 1300 °C. Samples BZT-b−e have comparable peak widths for the cubic (110) reflection at 2θ = 30.9°. After a pellet of sample BZT-b covered in identical powder is heated for 20 h at 1425 °C, the trigonal superstructure phase vanishes in BZT-c. In contrast, heating BZT-b as a pellet for 2 weeks at 1150 °C maintains the superstructure with an intensity ratio of 0.53(5), similar to that seen in BZT-d. The intensity ratio reaches a maximum of 0.83(6) in BZT-e, heated for 2 weeks at 1350 °C. Here, the superstructure peaks are also at their sharpest, corresponding to large (790(42) Å) domains. However, under these conditions a well-crystallized impurity phase is also formed. The preparation conditions for BZT-e are comparable with the method reported by Jacobson et al.[5] The powder X-ray diffraction pattern for BZT-e is very similar to patterns for commercial samples with excellent dielectric properties.[13] These results illustrate the complex processes involved in the synthesis of trigonal BZT phases. If samples are not covered during synthesis (d and e versus c), B-cation ordering persists at 1150 °C (BZT-d) and strong evidence of increased B-cation ordering is observed at 1350 °C (e). Prolonged heating of uncovered samples at an intermediate temperature, 1150 °C, maintains the pure BZT phase whereas the same reaction at 1350 °C leads to the formation of an impurity and large trigonal cation-ordered domains. In contrast heating a covered sample at 1425 °C (BZT-c) shows almost no sign of cation ordering, the decrease in superstructure intensity compared to the parent sample by being presumably due to the decrease in the order parameter on approach to the 1600 °C order−disorder temperature for pure BZT.[14] Annealing in an open crucible leads to enhancement of the superstructure intensity at either lower or higher annealing temperatures than those used for BZT-b,

(12) Larson, A. C.; von Dreele, R. B. *General Structure Analysis System*; Los Alamos National Laboratory Report LAUR 86-748 (2000); Los Alamos National Laboratory: Los Alamos, NM, 2000.

(13) Iddles, D., personal communication.

(14) Qazi, I.; Reaney, I. M.; Lee, W. E. *J. Eur. Ceram. Soc.* **2001**, *21*, 2613−2616.

presumably due to a higher thermodynamic value of the order parameter in the first case and superior ordering kinetics in the second case. The growth of the 790(42) Å superstructure domains together with the formation of an impurity phase in BZT-e is also noteworthy. BZT forms at 1100 °C in BZT-a where, surprisingly, some cation ordering is also found.

Characterization of the Impurity Phase. The crystalline impurity phase observed in BZT-e and the powder form of BZT-f is commonly observed in BZT samples that are not covered and protected against ZnO loss during preparation, suggesting it to be a Zn-deficient phase. None of the previously proposed impurities, $BaTa_2O_6$[15] and $Ba_3Ta_2O_8$,[7] nor other known phases in the Ba−Ta−O system such as $Ba_4Ta_2O_9$ were found to match the extra peaks observed. Tolmer and Desgardin[15] report another possible phase that is isotypic with $Ba_4LiTa_3O_{12}$,[16] where the two Li^+ ions occupying an octahedral site are replaced by one Zn^{2+} ion and one vacancy. This would give an impurity with composition $Ba_8ZnTa_6O_{24}$. The $P6_3/mmc$ structure (a = 5.82138(3) Å, c = 19.0606(2) Å) indexes all the impurity reflections in the BZT-f powder sample. It comprises fully occupied corner-sharing TaO_6 octahedra (Ta on site 4f) with face-sharing metal−oxygen octahedra (site 4e) randomly occupied by Ta (occupancy = $^1/_2$), Zn (occupancy = $^1/_4$), and vacancies (occupancy = $^1/_4$). This cation distribution also minimizes the electrostatic repulsion between Ta^{5+} across the shared octahedral faces. However, Abakumov et al. report a Ni analogue $Ba_8NiTa_6O_{24}$ which is also hexagonal (a = 10.08297(6) Å, c = 19.0605(2) Å in BZT-f powder) in the noncentrosymmetric space group $P6_3cm$.[17] In this case the vacancies on the face-sharing octahedra are ordered to produce two different pairs of face-sharing octahedra, giving rise to the $\sqrt{3}$ increase of the a lattice constant. Both structures show good agreement with the observed impurity phase. The impurity intensities when used in Rietveld analysis of the multiphase mixtures constitute only some 10 wt % of the powder sample f. This and the significant preferred orientation that is observed in the X-ray pattern, in agreement with the reported platelike habit of the phases, prevent an unambiguous structural characterization being obtained from these data. However, we have isolated single-phase material of this "8−1−6" stoichiometry which adopts the in-plane supercell and will report on this fully in a separate publication.

In previous publications similar impurity peaks are observed in tantalates and niobates,[8,10,18,19] suggesting that the formation of this phase is common with this class of B-site ordered early transition metal perovskites. The correct identification and characterization of this impurity is particularly important since there is significant peak overlap between the impurity phase reflections and those of BZT. A powder diffraction pattern collected over the range 0.89 ≤ d/Å ≤ 5.9 collected on a medium-resolution powder X-ray diffractometer shows only some 6 BZT peaks that are well-separated from those of the impurity phase. The presence of this phase can therefore significantly affect intensity ratios and conclusions drawn concerning extent of B-site order.

Table 2. Cation Compositions of BZT-f in Pellet and Loose Powder Prepared from Stoichiometric Starting Materials for $Ba_3ZnTa_2O_9$

	Ba	Zn	Ta
pellet	3	0.93(1)	1.94(1)
powder	3	0.84(1)	1.99(1)

The cation concentrations were normalized with respect to Ba.

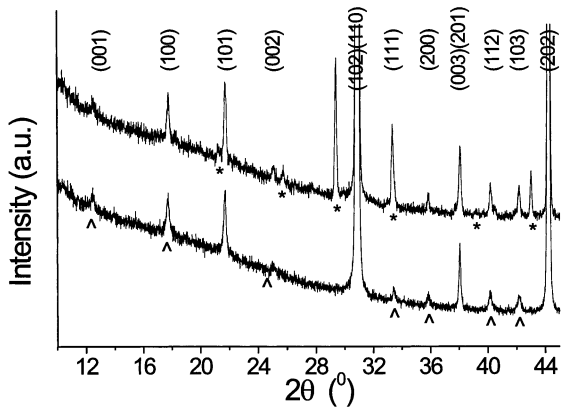

Figure 3. Laboratory X-ray data (λ = 1.54059 Å) for BZT-f in pellet (lower trace) and powder (upper trace) form. ∧ indicates superstructure peaks and * denote the impurity phase peaks. Miller indices correspond to the trigonal supercell.

Crystal Structures of the Annealed Samples. The overall composition of the pelletized and powder forms of BZT-f was determined by X-ray fluorescence spectroscopy. The cation compositions listed in Table 2 indicate significant levels of ZnO loss during preparation. In particular, the loose powder showed a large, 16 atom %, loss of Zn, whereas the loss for the pellet is 7 atom % Zn. The Ta loss is significantly lower with values between 0.5 and 3 atom %. It was also established that powders with an initial excess of 2 mol % of ZnO resulted in the same cation compositions as the stoichiometric starting material after annealing. This indicates that excess ZnO is easily removed by means of evaporation, whereas the ZnO lost from the BZT phase volatilizes at a significantly slower rate.

The laboratory powder X-ray diffraction patterns for the pellet and the loose powder are shown in Figure 3. All the peaks of the pelletized sample can be indexed on the trigonal ordered BZT unit cell, whereas the loose powder shows additional peaks due to the same impurity found for BZT-e. Preliminary analysis of the widths of the (100) superstructure reflections suggests that the pellet and the powder have differently sized trigonal domains of 375(11) and 696(22) Å, respectively. The fits for the (100) superstructure reflection are shown in Figure 4, with the parameters given in Table 1. The cation ordering in the powder sample as determined from the intensity ratio IR appears to be lower than that in the pellet due to systematic errors arising from overestimation of the (110) intensity in the powder, which is enhanced by the $Ba_8ZnTa_6O_{24}$ impurity phase.

(15) Tolmer, V.; Desgardin, G. *J. Am. Ceram. Soc.* **1997**, *80*, 1981−1991.
(16) Collins, B. M.; Jacobson, A. J.; Fender, B. E. F. *J. Solid State Chem.* **1974**, *10*, 29−35.
(17) Abakumov, A. M.; van Tendeloo, G.; Scheglov, A. A.; Shpanchenko, R. V.; Antipov, E. V. *J. Solid State Chem.* **1996**, *125*, 102.
(18) Kim, I.-T.; Hong, K. S.; Yoon, S.-J. *J. Mater. Sci.* **1995**, *30*, 514−521.
(19) Vincent, H.; Perrier, C.; l'Heritier, P.; Labeyrie, M. *Mater. Res. Bull.* **1993**, *28*, 951−958.

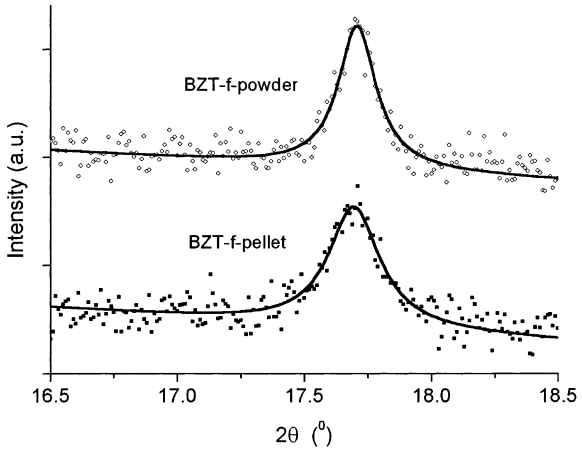

Figure 4. Laboratory X-ray data comparing the (100) superstructure peaks for BZT-f pellet (lower) and powder (upper). The solid lines are best fits using a single pseudo-Voigt function.

The trigonal domains for the pellet (375(11) Å) are considerably smaller than those found for the powder (D = 696(22) Å), consistent with the TEM studies. The powder and pellet samples have previously defined IR intensity ratios of 0.89(3) and 0.78(3), respectively, making them comparable in extent of order with "fully ordered" BZT phases studied previously.[5,7]

Electron Microscopy. The ordering of single layers of Zn^{2+} octahedral B site cations alternating with double layers of Ta^{5+} cations occurs perpendicular to a ⟨111⟩-type direction of the cubic subcell. Since there are four distinct ⟨111⟩ directions in a cubic lattice (i.e., [1 1 −1], [−1 1 1], [1 1 1], and [1 −1 1]), the superlattice ordering should have an equal probability of occurring along any of these directions, thus giving rise to four crystallographically equivalent orientational domains (P, Q, R, and S). Faulting in the Zn−Ta−Ta−Zn ordering sequence along the selected ⟨111⟩ direction within a domain can also give rise to antiphase domains.[14] The physical size of the domains formed can be directly visualized by lattice imaging the material along a certain specific direction (e.g., ⟨110⟩ and ⟨100⟩ as referred to the original cubic unit cell). This is illustrated in Figure 5a,b for the pellet and powder samples of BZT-f imaged along the {110} cubic subcell direction. The domain sizes are about 10−15 nm for the pellet and 50−100 nm for the powder sample in the crystallites studied.

In Figure 5a, the small domains of the pellet sample are clearly visible, there are three distinct types of contrast. The two regions labeled P and Q show strong fringes which rotate by an angle of 110° on crossing the domain boundary, consistent with ordering along different ⟨111⟩ directions. The third type of region, labeled RS, shows no evidence of superlattice fringes at all. Fourier transforms (FT's) obtained from the localized domains marked P, Q, and RS are shown in parts a, b, and c of Figure 6, respectively, along with a FT (Figure 6d) generated from the whole area shown in Figure 5a. It is clear that in the domains P and Q, superlattice reflections are present at $^1/_3$ [111] in the cubic subcell since the Zn^{2+} and Ta^{5+} 1:2 ordered layers are edge-on in this projection. These correspond to the [100] and [010] trigonal zone axes in which superstructure reflections are expected. For domain RS the superlattice ordering direction is inclined with respect to the incident electron beam so the Zn^{2+} and Ta^{5+} cation columns appear mixed (or random) in projection, corresponding

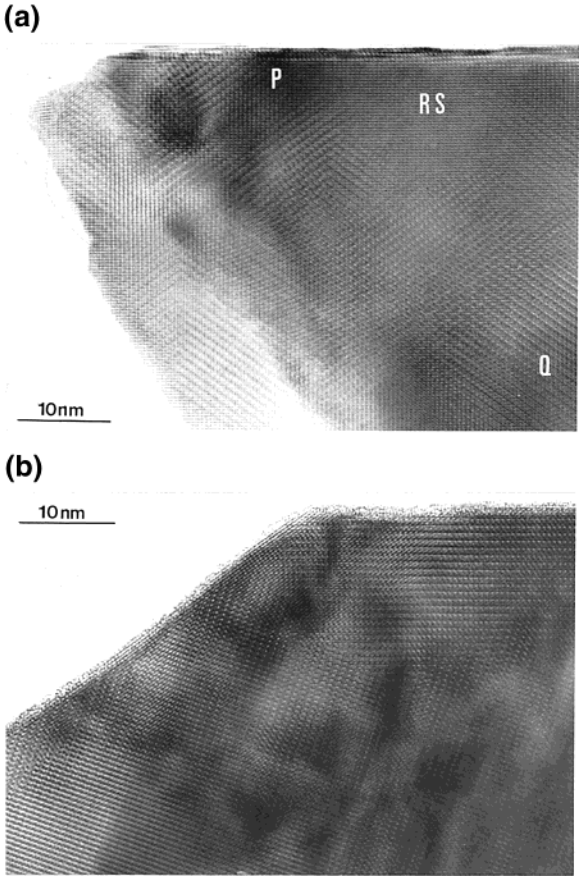

Figure 5. Lattice images of (a) pellet BZT-f and (b) powder BZT-f along the ⟨110⟩ direction of the cubic subcell.

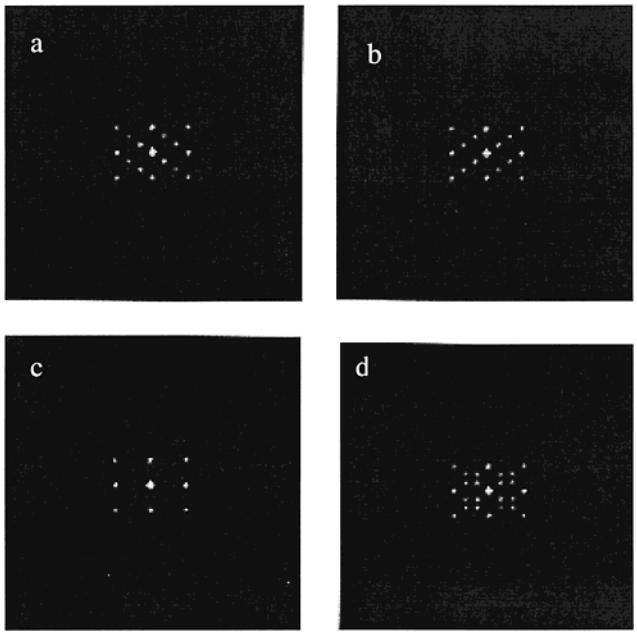

Figure 6. Fourier transforms (FTs) of pellet BZT-f obtained from the localized domains marked P, Q, and RS are shown in (a), (b), and (c) respectively, along with an FT ((d)) generated from the whole area shown in Figure 5a. Note the differing orientation of the cation-induced superstructure reflections in (a) and (b) and their absence in (c).

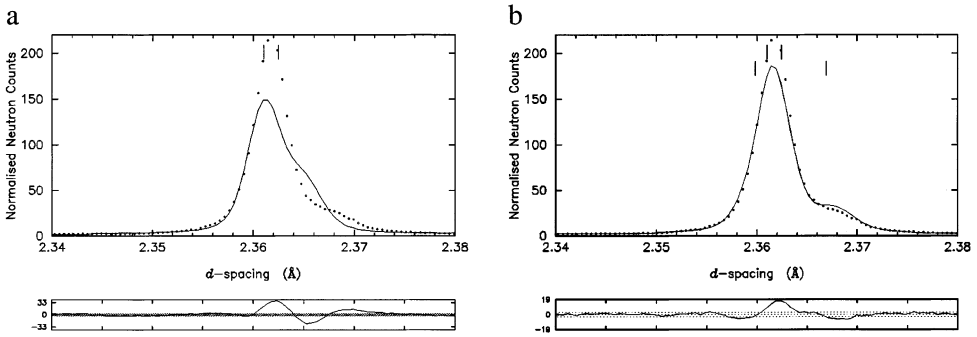

Figure 7. Section of the Rietveld refinement for the neutron time-of-flight data for the BZT-f pellet sample using a structural model comprising (a) a single trigonal phase and (b) two trigonal phases. Upper tick marks correspond to the calculated peak positions for phase 2 and the lower tick marks to phase 1.

Table 3. Data Collection Details for the Pelletized BZT-f Sample

	X-ray	Neutron	X-ray	X-ray
histogram no.	1	2	3	4
λ (Å)	1.54059	1.2−5.2	1.54059	1.000057
no. profile points	10990	3659	2997	8031
2θ range, step (deg)	10−120, 0.01	⟨168⟩	10−49, 0.01	40−80, 0.005
d-spacing range (Å)	0.81−8.84	0.82−2.5	0.98−8.84	0.99−1.47
excluded regions	0	0	3	0

to the [112] trigonal zone axis in which only the cubic subcell reflections are visible.

Rietveld Refinement of Pelletized $Ba_3ZnTa_2O_9$. The multiple occupancy (by Zn, Ta, and cation vacancies) of each of the two crystallographically distinct B-cation sites in the BZT ordered structure cannot be determined unambiguously using a single powder diffraction data set. To determine reliably all B-cation occupancies, diffraction patterns with at least three different independent sets of neutron scattering lengths and/or X-ray form factors are needed. This requires the analysis of resonant powder X-ray diffraction data collected at several X-ray absorption edges, which is underway and will be published elsewhere. In the present studies the phase composition and crystallographic structures of the constituent phases in the pelletized sample were modeled and refined against four histograms of data, as summarized in Table 3. The first histogram is a laboratory X-ray diffraction data set recorded for 13 h and the second is high-resolution time-of-flight neutron diffraction data collected on the back-scattering detector bank of HRPD. The third histogram is laboratory X-ray diffraction data collected for 3 days over the low-angle region. These data provide a much better description of the supercell peaks arising from the 2:1 cation ordering and all regions of the pattern containing subcell peaks were excluded from this histogram. The fourth histogram is the synchrotron data.

Initial inspection of the fits and agreement indices based on the accepted literature model of BZT appeared satisfactory; however, on closer examination substantial deficiencies were apparent. Whereas medium-resolution powder X-ray diffraction data agree well with a single-phase BZT model, high-resolution X-ray and neutron diffraction data reveal broad shoulders observed for a large number of peaks (see Figure 7). A satisfactory fit to all four histograms was obtained subsequently with a model consisting of two trigonal BZT phases. The shoulders were assigned to Phase 1, which has the larger unit cell volume of 205.854(2) Å^3 and exhibits a broader peak profile than Phase 2 which has a unit cell volume of 205.788(3) Å^3.

Initially, a total of 68 background parameters were refined for all four histograms but held fixed during later refinement cycles. The backgrounds of all the X-ray patterns were described using a cosine Fourier series, while a power series was used for the time-of-flight neutron diffraction data. The peak profile parameters for all four histograms were refined together with the histogram scale factors. Surface roughness terms according to Pitschke[20] were refined for the X-ray data and for the neutron data an absorption correction for a cylindrical sample was applied. These parameters were fixed for subsequent refinements. Phase fractions were constrained to be the same for all X-ray histograms, whereas the neutron-derived phase fractions were refined independently to allow for the different sample penetration depths of the respective radiation. The occurrence of two BZT phases in the sample introduces parameter correlation into the refinements and requires the use of various constraints at different stages of the refinement process. Initially, a model comprising two fully ordered phases was refined with all equivalent positional parameters between the two phases constrained to be equal and isotropic displacement parameters for all atoms. The refinement converged but yielded an anomalously large negative displacement parameter for Zn. The residuals ($\chi^2 = 2.59$) for this model are significantly larger than those for the more complex models refined subsequently (Table 4). The largest discrepancy is found for histogram 3, which only contains the superstructure reflections. The Rietveld fits with this fully ordered model are shown in Figure 8. It is clear that the broader Phase 1 is very poorly fitted in comparison with the subsequent refinements.

Once the presence of two distinct BZT phases in the pellet sample was established, the issue of the differences between the two phases, in terms of the degree of cation site order and the Zn loss indicated by X-ray fluorescence measurements, was addressed. The data presented here only have two sets of scattering factors for the constituent elements, namely, the neutron scattering lengths for the HRPD data and nonresonant form factors for all powder X-ray diffraction data, and therefore all site occupancies cannot be refined freely.

(20) Hermann, H.; Pitschke, W.; Mattern, N. *Phys. Status Solidi A* **1992**, *132*, 103−114.

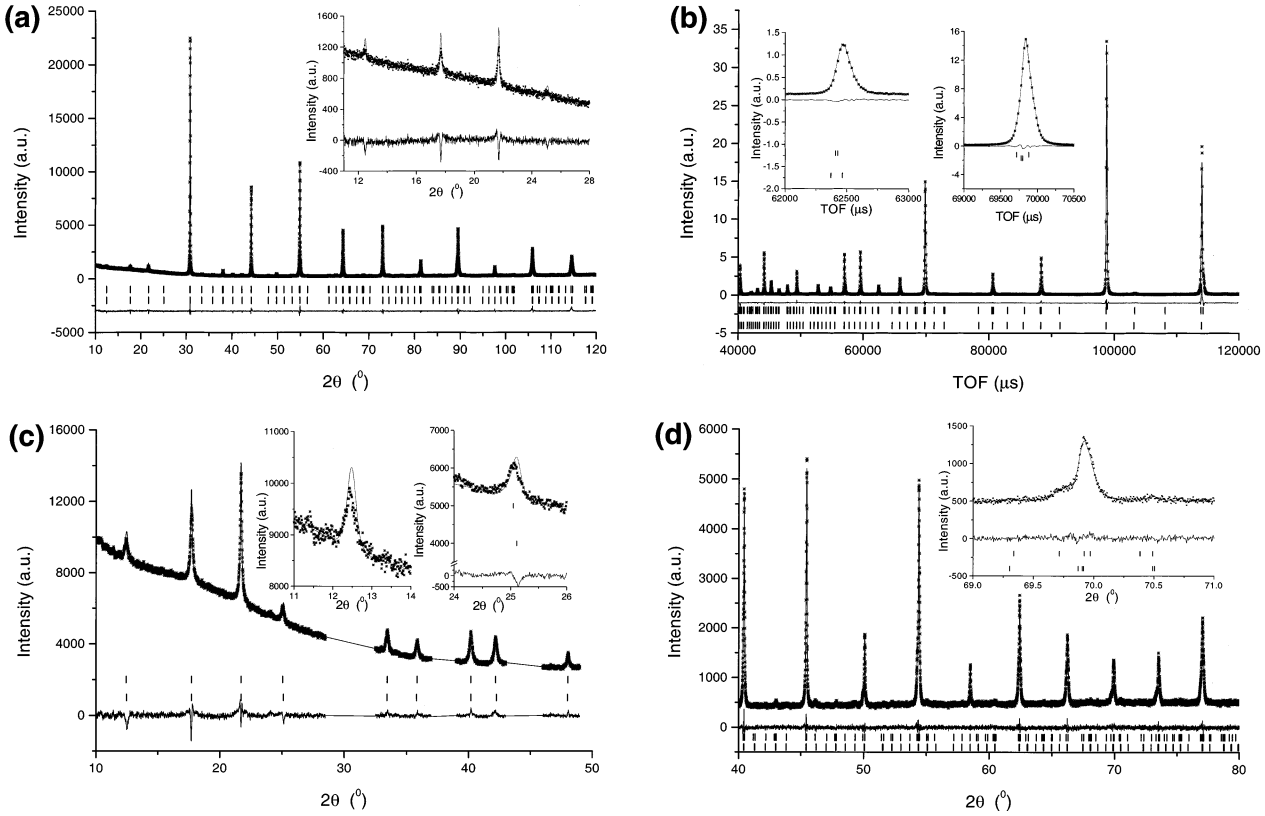

Figure 8. Profile fits for the Rietveld refinement of the BZT-f pellet sample assuming fully occupied and fully ordered B-cation lattices for both hexagonal phases. (a) Histogram 1, laboratory X-ray data ($\lambda = 1.54059$ Å); (b) histogram 2, high-resolution neutron time-of-flight; (c) histogram 3, low-angle laboratory X-ray data ($\lambda = 1.54059$ Å); (d) histogram 4, synchrotron X-ray ($\lambda = 1.000057$ Å). Lower tick marks correspond to the calculated peak positions for phase 1 and the upper tick marks to phase 2.

Table 4. Agreement Indices for Various Two-Phase Models for the Pelletized BZT-f Sample

	histogram no.											
	1		2		3		4		combined			
model	R_{wp} (%)	R_p (%)	R_{wp} (%)	R_p (%)	R_{wp} (%)	R_p (%)	R_{wp} (%)	R_p (%)	R_{wp} (%)	R_p (%)	χ^2	no. of variables
1: fully ordered trigonal 2: fully ordered trigonal	6.69	4.97	7.00	5.80	3.29	1.77	4.70	3.73	4.73	2.76	2.59	13
1: fully ordered trigonal 2: fully disordered trigonal	6.42	4.83	5.75	5.31	1.85	1.38	4.55	3.57	3.97	2.45	1.83	13
1: fully ordered trigonal 2: fully disordered cubic	6.55	4.93	6.35	5.73	2.34	1.53	4.65	3.64	4.25	2.58	2.09	13
final refinement	6.42	4.86	5.72	5.13	1.69	1.31	4.54	3.56	3.93	2.41	1.77	19

The Ta stoichiometry was fixed at 2.00 for both phases and in all refinements and initially occupation factors for the B-cations were then refined with constraints, imposing 2:1 Ta:Zn stoichiometry. The fit to the data was improved significantly by allowing the extent of Zn/Ta cation order to differ between the two phases. Assuming a fully ordered phase 1 and fully disordered phase 2 reduces χ^2 from 2.56 to 1.83 and on refining the degree of site order this improves further to 1.79. At this stage refinements were also carried out modeling phase 2 as a disordered cubic phase. These refinements are stable but with poorer fits across all histograms yielding a χ^2 figure of 2.09. This is a key distinction as it demonstrates that both phases have Zn/Ta site order, as this drives the trigonal symmetry. The Zn occupancy on each site in the two BZT phases was then refined independently of the Ta occupancy, for consistency with the XRF data, indicating that Zn is lost and the diffraction data which show that only BZT phases are present. This results in a minor improvement to the fits, χ^2 decreasing to 1.77, and the indication that Zn loss is confined to the less-well-ordered phase 2. Analysis of the multihistogram diffraction data therefore leads to the conclusion that the B-cation sites in the broader phase 1 are fully ordered and fully occupied, while the sharper phase 2 shows a large degree of cation disorder on the B-sites and also the presence of Zn cation vacancies.

Another model was tested where the constraints on positional parameters between the two phases were removed, giving a total of 24 variable parameters (including B-cation occupancies, phase fractions, and unit cell parameters). No significant improvements to the fit or differences between the atomic coordinates of the phases were observed. The final Rietveld refinement results, with constrained atomic coordinates and isotropic thermal parameters for oxygen, are summarized in Table 5 and the agreement factors are summarized in Table 4. Bond lengths and bond angles common for both phases are given in Table 6. The final Rietveld refinement profile fits are shown in Figure 9. The refined overall composition of the pellet sample is Ba_3-

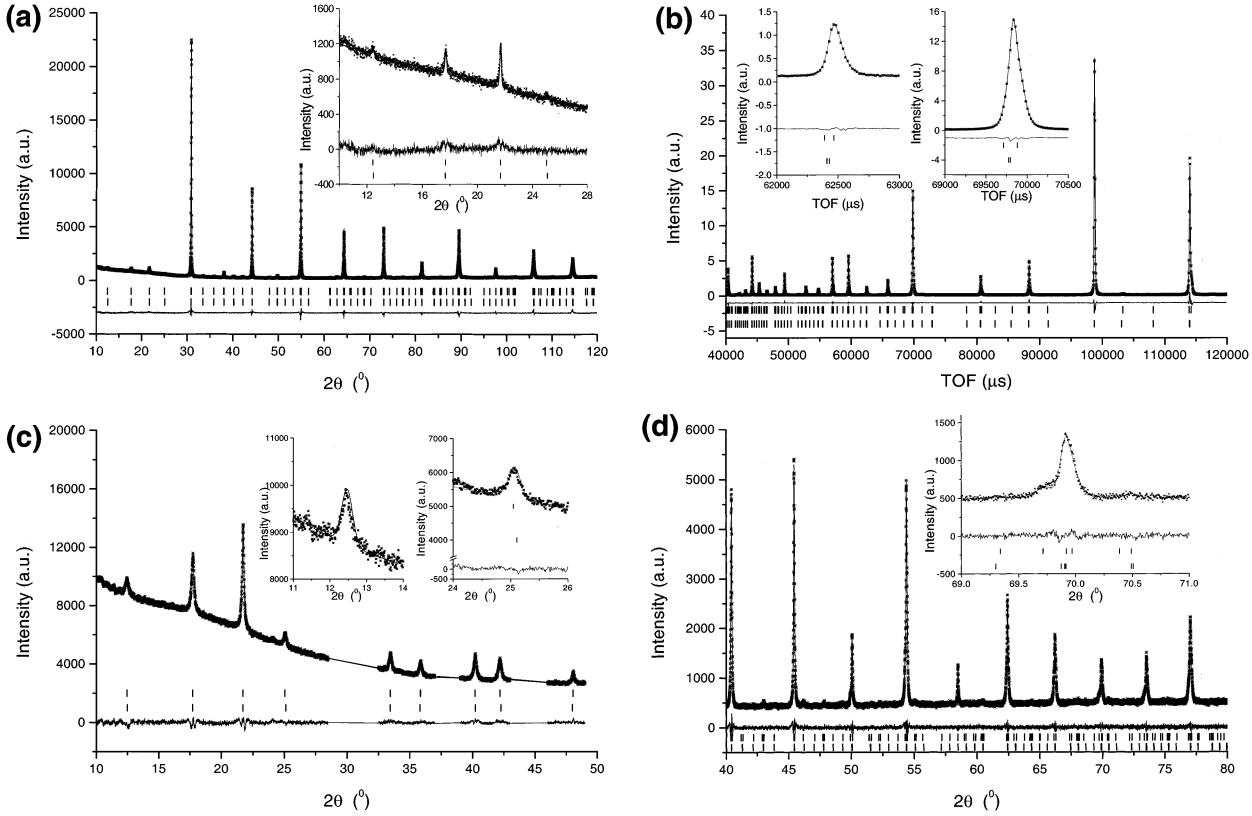

Figure 9. Final profile fits for the Rietveld refinement of the BZT-f pellet sample. (Histogram labeling as in Figure 8.)

Table 5. Refined Structural Parameters for the Two BZT Phases in the Pelletized BZT-f Sample[a]

	site	*x*/*a*	*y*/*b*	*z*/*c*	occup.	$U_i/U_e \times 100$
Ba(1)	2d	1/3	2/3	0.6622(1)	1	0.73(1)
Ba(2)	1a	0	0	0	1	0.73(1)
Ta(1)	2d	1/3	2/3	0.1739(2)	1.008(1)	0.26(2)
					0.78(1)	0.26(2)
Zn(2)	1b	0	0	1/2	1.012(6)	0.41(6)
					0.53(4)	0.41(6)
Zn(1)	2d	1/3	2/3	0.1739(1)	−0.024(4)	0.26(2)
					0.18(2)	0.26(2)
Ta(2)	1b	0	0	1/2	−0.015(2)	0.41(6)
					0.44(2)	0.41(6)
O(1)	3e	1/2	0	0	1	0.89(1)
O(2)	6i	0.1706(1)	−0.1706(1)	0.3264(2)	1	0.89(1)

[a] Upper line BZT-f1 "broad"; lower line BZT-f2 "sharp". Space group: $P\bar{3}m1$. Lattice constants: BZT-f1, $a = 5.78299(2)$ Å, $c = 7.10761(6)$ Å; $V_c = 205.854(2)$ Å^3. BZT-f2, $a = 5.78810(3)$ Å, $c = 7.09283(8)$ Å; $V_c = 205.788(3)$ Å^3. Stoichoimetry and phase fraction (wt %): BZT-f1, $Ba_3Zn_{1.00(1)}Ta_{2.00}O_9 = 54.7(2)$; BZT-f2 $Ba_3Zn_{0.89(1)}Ta_{2.00}O_9$ 45.3(2). The Ta order parameter $(n_{Ta}(2d) - n_{Ta}(1b))/(n_{Ta}(2d) + n_{Ta}(1b)) = 1.030(6)$ and 0.27(3) in the broad and sharp phases, respectively. The Zn order parameter $(n_{Zn}(1b) - n_{Zn}(2d))/(n_{Zn}(2d) + n_{Zn}(1b)) = 1.05(2)$ and 0.5(1). This yields a mean order parameter, weighted by the phase fractions, of 0.69(8) (Ta) and 0.8(2) (Zn).

$Zn_{0.95(1)}Ta_{2.00}O_9$, with the extent of zinc loss agreeing well with the XRF data.

The refined cation site occupancies allow the definition of order parameters for the extent of 2:1 ordering based on the Ta and Zn occupancies of the two symmetry-inequivalent cation sites in the $P\bar{3}m1$ space group (Table 5). The errors for the site occupancies should be considered with caution due to strong correlations between the two similar phases. The reported statistical errors for the occupancies are therefore likely to be underestimated. Similarly, it should be noted that, despite the observed B-cation deficiency, the model for phase 2 is refined assuming fully occupied oxygen sites. On the basis of the cation occupancies and charge balance, 1.2 mol % of oxygen deficiency is required. The data are not sensitive to this level of O deficiency. Fixing the O occupancies at this value simply results in a reduction of the oxygen displacement parameter by 6% without affecting the goodness of fit.

Table 6. Interatomic Distances and Angles Determined from the Refined Structural Parameters for BZT Phases in the BZT-f Pelletized Sample[a]

		(Å)			(deg)
×3	Ba(1)−O(1)	2.9252(1)	×3	O(1)−Ba(1)−O(2)	179.597(1)
×3	Ba(1)−O(2)	2.8900(1)	×6	O(1)−Ba(1)−O(2)	89.093(1)
×6	Ba(1)−O(2)	2.8929(1)	×3	O(2)−Ba(1)−O(2)	176.461(1)
×6	Ba(2)−O(1)	2.8915(1)	×6	O(2)−Ba(1)−O(2)	90.917(1)
×6	Ba(2)−O(2)	2.8805(1)	×3	O(2)−Ba(2)−O(2)	180.000(1)
			×12	O(1)−Ba(2)−O(2)	89.999(1)
			×3	O(1)−Ba(2)−O(1)	180.00
×3	Ta−O(1)	2.0782(1)	×3	O(1)−Ta−O(1)	88.164(1)
×3	Ta−O(2)	1.9521(1)	×3	O(1)−Ta−O(2)	177.007(1)
	mean Ta−O	2.0151	×6	O(1)−Ta−O(2)	89.687(1)
	rms Ta−O	0.089	×3	O(2)−Ta−O(2)	92.385(1)
×6	Zn−O(2)	2.1052(1)	×6	O(2)−Zn−O(2)	89.163(1)
			×3	O(2)−Zn−O(2)	180.000(1)
			×6	O(2)−Zn−O(2)	90.837(1)

[a] The mean Ta−O distance at the 2d Ta site, and the standard deviation from this mean, is also quoted.

Rietveld Refinement of the $Ba_3ZnTa_2O_9$ Powder. The loose powder covering the pelletized sample was studied with laboratory powder X-ray and powder neutron diffraction (Table 7). The sample contains the $Ba_8ZnTa_6O_{24}$ impurity which was also modeled, for pragmatic reasons described above, using the simpler fully disordered structure in space group $P6_3/mmc$. Initially, the data were analyzed assuming the presence

Table 7. Refinement and Data Collection Details for Powder X-ray and Neutron Diffraction Data for the BZT-f Powder Sample[a]

	X-ray	Neutron
histogram no.	1	2
λ (Å)	1.54059	1.2−5.2
no. of profile points	10498	4403
2θ range (deg), step	15−120, 0.01	⟨168⟩
d-spacing range (Å)	0.81−5.90	0.67−2.5
excluded regions	0	0
R_{wp} (%)	5.99	7.14
R_p (%)	4.61	6.24

[a] For the three-phase refinement combined $R_{wp} = 6.56\%$, $R_p = 4.64\%$; $\chi^2 = 2.81$ for 33 variables.

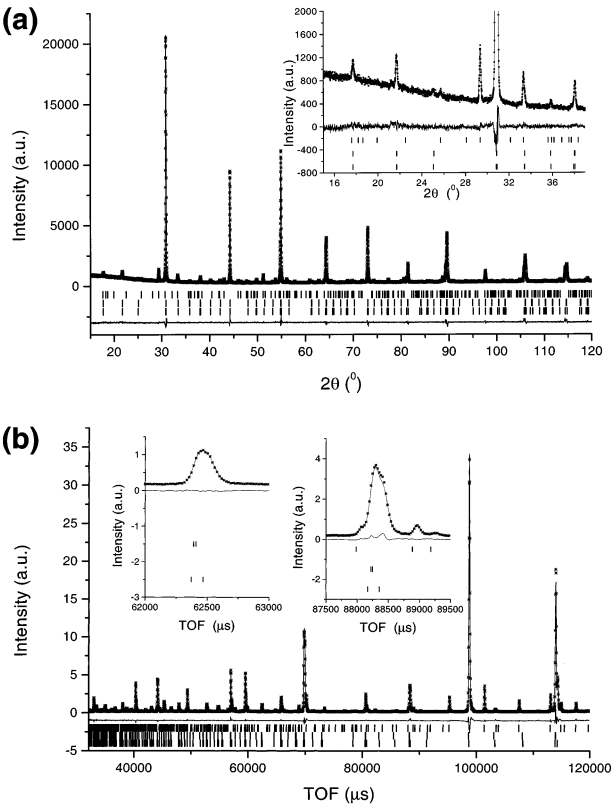

Figure 10. Final profile fits for the Rietveld refinement of the BZT-f powder sample. (a) Histogram 1, laboratory X-ray data ($\lambda = 1.54059$ Å); (b) histogram 2, high-resolution neutron time-of-flight. Upper tick marks correspond to the calculated peak positions for $Ba_8ZnTa_6O_{24}$, middle tick marks to BZT phase 1, and lower tick marks to BZT phase 2.

of two phases, namely, the impurity and a single ordered BZT phase. However, the high-resolution powder neutron diffraction data clearly indicate that more than one BZT phase is present, as found for the pelletized sample, and so a similar refinement strategy was adopted. Two BZT phases, differing in their B-site cation ordering, unit-cell constants, and peak widths but with the same positional parameters, were refined (Figure 10). Phase fractions were not constrained to be the same in the X-ray and neutron diffraction patterns, but the refined phase fractions are very similar for the two histograms (<4 wt % difference). The parameters of the two BZT phases are again strongly correlated and with only two histograms of data available Zn and Ta displacement parameters were constrained to be equal. The data clearly support a model comprising an ordered phase 1 and a disordered phase 2 ($\chi^2 = 2.88$) over a model using two ordered phases ($\chi^2 = 2.95$). Subsequent refinement

Table 8. Refined Structural Parameters for the Three Phases in the BZT-f Powder Sample

	site	x/a	y/b	z/c	occup.	$U_i/U_e \times 100$
Ba(1)	2d	$^1/_3$	$^2/_3$	0.6622(3)	1	0.89(1)
Ba(2)	1a	0	0	0	1	0.89(1)
Ta(1)	2d	$^1/_3$	$^2/_3$	0.1741(3)	1.00(1)	0.59(1)
					0.75(4)	0.59(1)
Zn(2)	1b	0	0	$^1/_2$	1.01(1)	0.59(1)
					0.50(7)	0.59(1)
Zn(1)	2d	$^1/_3$	$^2/_3$	0.1741(3)	0.00(1)	0.59(1)
					0.25(4)	0.59(1)
Ta(2)	1b	0	0	$^1/_2$	−0.01(1)	0.59(1)
					0.50(7)	0.59(1)
O(1)	3e	$^1/_2$	0	0	1	1.02(1)
O(2)	6i	0.1714(1)	−0.1714(1)	0.3252(2)	1	1.02(1)

[a] The phase fractions are based on the powder X-ray data. The neutron data yielded phase fractions deviating 2−4% from the X-ray results. BZT-1 denotes the broad BZT phase and BZT-2 the sharp phase. Space group: $P\bar{3}m1$. Lattice constants: BZT-1, $a = 5.78277(2)$ Å, $c = 7.10845(6)$ Å; $V_c = 205.827(2)$ Å^3. BZT-2, $a = 5.78883(1)$ Å, $c = 7.08588(3)$ Å; $V_c = 205.639(3)$ Å^3. Stoichiometry and phase fraction (wt %): BZT-1, $Ba_3ZnTa_2O_9 = 63.4(2)$; BZT-2, $Ba_3ZnTa_2O_9 = 26.5(2)$. Impurity phase $Ba_8ZnTa_6O_{24}$ phase fraction (wt %): 10.1(2). Lattice constants: $a = 5.82138(3)$ Å, $c = 19.0606(2)$ Å; $V_c = 559.394(6)$ Å^3. The Ta order parameter $(n_{Ta}(2d) - n_{Ta}(1b))/(n_{Ta}(2d) + n_{Ta}(1b)) = 1.02(4)$ and 0.20(2) in the broad and sharp phases, respectively. The Zn order parameter $(n_{Zn}(1b) - n_{Zn}(2d))/(n_{Zn}(2d) + n_{Zn}(1b)) = 1.00(2)$ and 0.3(1). This yields a mean order parameter, weighted by the phase fractions, of 0.8(1) (Ta) and 0.8(3) (Zn).

Table 9. Interatomic Distances and Angles Determined from the Refined Structural Parameters for the BZT Phases in the BZT-f Powder Sample[a]

		(Å)			(deg)
×3	Ba(1)−O(1)	2.9293(13)	×3	O(1)−Ba(1)−O(2)	179.321(1)
×3	Ba(1)−O(2)	2.8921(26)	×6	O(1)−Ba(1)−O(2)	88.90(6)
×6	Ba(1)−O(2)	2.8933(1)	×3	O(2)−Ba(1)−O(2)	176.461(1)
×6	Ba(2)−O(1)	2.8911(1)	×6	O(2)−Ba(1)−O(2)	91.13(6)
×6	Ba(2)−O(2)	2.8754(22)	×3	O(2)−Ba(2)−O(2)	180.000(1)
			×12	O(1)−Ba(2)−O(2)	89.999(1)
			×3	O(1)−Ba(2)−O(1)	180.00
×3	Ta(1)−O(1)	2.0827(13)	×3	O(1)−Ta−O(1)	87.91(7)
×3	Ta(1)−O(2)	1.9355(23)	×3	O(1)−Ta−O(2)	176.46(10)
	mean Ta−O	2.009	×6	O(1)−Ta−O(2)	89.55(4)
	rms Ta−O	0.105	×3	O(2)−Ta−O(2)	92.89(9)
×6	Zn(2)−O(2)	2.1246(22)	×6	O(2)−Zn−O(2)	88.95(8)
			×3	O(2)−Zn−O(2)	180.000(1)
			×6	O(2)−Zn−O(2)	91.05(8)

[a] The mean Ta−O distance at the 2d Ta site, and the standard deviation from this mean, is also quoted.

of the degree of cation ordering gives a marginal improvement to the fit and is stable, but introduces correlation with the extent of the Zn/Ta order between phases and prevents the assignment unambiguously of zinc deficiency to either phase. The final refined parameters given in Table 8 are not significantly different from models with fixed fully ordered and fully disordered cation sites in the two distinct BZT phases. However, both BZT phases are clearly trigonal (refinement with the second BZT phase as a cubic perovskite is markedly inferior), demonstrating at least partial cation order in the second phase. Bond length and angle values are given in Table 9.

The broader BZT-1 phase has more complete cation ordering than the sharper phase 2, as also found in the pellet sample. Considering the refined stoichiometries and phase fractions of all three phases reveals an overall Zn deficiency, corresponding to $Ba_3Zn_{0.94}Ta_{2.00}O_9$, with respect to the starting materials. This suggests a lower degree of Zn loss as compared with that shown in the

X-ray fluorescence results (Table 2) but simply reflects the insensitivity of the refinement to Zn deficiency in the BZT phases.

Discussion

Detailed analysis of high-resolution powder diffraction data shows that the sluggish cation-ordering kinetics in BZT and the tendency for ZnO loss at high temperature complicates the simple picture of enhanced domain size and extent of ordering within a domain as annealing proceeds, which is deduced from laboratory powder X-ray diffraction studies of BZT ordering. In both the powder and pellet samples, there are two BZT phases with different extents of cation order and resulting trigonal distortion, as monitored by the *c*/*a* ratio. Loss of ZnO is apparent in both samples, with extensive loss from the powder being accommodated by introduction of the Zn-deficient $Ba_8ZnTa_6O_{24}$ impurity phase into the phase assemblage: this Zn loss occurs together with the growth of larger domains of the ordered BZT phase. In the pellet sample, the phase fractions of the fully ordered and partly ordered phases are approximately equal. The extent of order in the two phases can be quantified via order parameters based on the Zn and Ta occupancy of the two distinct octahedral sites: the more ordered phase is completely ordered and has broader Bragg reflections than the less ordered phase, which has approximately 40% order. The differing extents of cation order in the two phases would be expected to drive different trigonal distortions, consistent with the *c*/*a* ratios of 1.2291 (ordered, broad) and 1.2254 (disordered, sharp) compared with 1.2247 for an undistorted ideal cubic disordered perovskite. The less ordered, sharper phase accommodates the extent of B-site vacancies present at the composition found for the pellet. The enhanced level of Zn loss observed in the powder cannot be tolerated as B-site vacancies in the perovskite structure and results in the formation of the impurity phase, where the face-sharing octahedral sites allow the accommodation of larger Zn deficiency. It is intriguing, and probably significant, that the better ordered phase has the larger unit cell volume, as cation ordering generally results in a reduction of the volume.[21] This volume enhancement in the more ordered phase can be related to Zn deficiency in the less ordered phase. This information from the cell parameters is consistent with the Zn deficiency identified from the Rietveld analysis in this phase and provides good supporting evidence for the final refined model.

The most obvious effects of the enhanced ZnO loss observed in the higher surface area powder sample are the appearance of the $Ba_8ZnTa_6O_{24}$ impurity to accommodate the Zn deficiency and the sharpening of the superstructure reflections due to an increase in the ordered domain size from 375 to 696 Å. The enhanced domain size correlates with a larger fraction of the ordered perovskite phase in the powder sample. The subcell reflection widths of the two BZT phases in the powder sample are closer to each other than those in the pellet, as the fully ordered phase is sharper and the disordered phase broader. These observations are consistent with the existence of the two BZT phases in both pellet and powder samples being closely related to the ordering process itself, as a mechanism of accommodating the ZnO loss which occurs under these processing conditions. The partially ordered phase has an almost pseudo-cubic *c*/*a* value of 1.2241, while the *c*/*a* ratio of 1.2292 in the ordered phase is very similar to that found for this phase in the pellet sample. The considerably reduced trigonal distortion in the partially ordered phase is consistent with the refined site occupancy order parameters. As for the pellet, the disordered phase has the smaller unit cell volume of the two BZT phases. The decrease in phase fraction and in the extent of order of the partially ordered phase as the 2:1 ordered domains in the fully ordered phase grow in size is consistent with the idea of the second, less ordered BZT phase acting as a "sink" during the ordering process as the fully ordered phase develops. Although the intensity data do not allow the question of Zn occupancy to be addressed directly, the reduced cell volume of the disordered phase, as in the pellet, is consistent with any Zn vacancies in the perovskite structure being located in this phase. Thus, the refined Zn occupancy, the *c*/*a* ratio, and the cell volume are all consistent with the development of a 2:1 ordered BZT phase being accelerated by zinc loss at the expense of a less ordered phase which can accommodate a low level of B-site Zn vacancies. These B-site vacancies may be involved in accelerating the ordering process by facilitating cation diffusion. The *c*/*a* ratio and extent of order in the fully ordered phase are very similar in both the pellet and powder samples, suggesting that the ordering involves the growth of this phase via rearrangement accommodated within the second more cation-disordered phase which supports any Zn deficiency.

This model is consistent with the observation of two BZT phases with different phase fractions in both samples, with the completely ordered phase being identical as judged by the *c*/*a* ratio and extent of cation order. It is important to note that the high-resolution diffraction data can only be modeled with two phases and that both phases support cation order, as they are trigonal rather than cubic. The complexity of the cation ordering is indicated by the observation that although the superstructure reflections are sharper in the powder sample, the integrated intensity is reduced compared with those in the pellet. This is because of (i) the influence of the impurity phase, (ii) the second phase being less ordered in the case of the powder, and (iii) the influence of Zn vacancies on the superstructure intensities. This demonstrates that it is dangerous to use the intensity of one superstructure reflection to evaluate the extent of order in such a complex system. This type of information is only accessible via quantitative analysis of diffraction data. Moreover, it complements electron diffraction and lattice imaging information available over much shorter length scales from TEM studies in that it is possible here to quantify the extent of Zn/Ta ordering and vacancy concentration within the ordered domains.

The rate of cation-ordered domain growth is related to the formation of the Zn-deficient impurity in the powder sample; the formation of this impurity is not a prerequisite for ordering, as the same ordering proceeds

(21) Woodward, P.; Hoffmann, R. D.; Sleight, A. W. *J. Mater. Res.* **1994**, *9*, 2118−2127.

more slowly in the pellet at the same temperature. The Zn loss does however appear to accelerate the formation of a larger fraction of the fully ordered phase. Similar *c*/*a* ratios of the ordered phases in the pellet and powder samples do suggest that both samples consist of very similar fully ordered phases in which the unit-cell level structure is comparable within the domains while the extent of the domains is larger in the powder sample. However, the changed *c*/*a* ratios in the partially ordered phases indicate that, within the ordered domains, these phases differ significantly and change as the extent of ordering and zinc loss increases. This well-defined difference in the partially ordered phases in the two samples suggests that the less-ordered phase acts sacrificially during the ordering process. In nucleation and growth models for the formation of ordered superstructures, the ordered and disordered phases ideally coexist during the ordering process. In this case, there are two coexisting phases with differing extents of order. The essentially fully ordered phase grows in spatial extent and phase fraction during the annealing process but the second phase is not simply a disordered matrix out of which order emerges. In both samples the second phase is considerably less ordered and may accommodate any zinc deficiency that is present. Most importantly, it changes significantly depending on the spatial extent of order within the main phase.

The bond lengths derived from the Rietveld refinement average over the two phases observed (as well as over the coherent scattering volume) and thus do not allow them to be distinguished directly. The 2:1 layered ordering motif is driven by the formation of two crystallographically distinct cation sites to accommodate the stereochemical preferences of the d^{10} Zn^{2+} and d^0 Ta^V cations. In both the pellet and powder samples the mean metal−oxygen distances are shorter at the predominantly Ta-occupied 2d site than at the predominantly Zn-occupied 1b site. Significantly, the difference between these mean bond lengths increases from 0.09 Å in the pellet to 0.12 Å in the powder. The increased distinction between the averaged environment of the two sites is consistent with more complete ordering between Zn and Ta in the powder sample. The Zn^{2+} cations occupy centrosymmetric sites while the enhanced tendency for Ta−O multiple bonding is reflected in the noncentric environment at the Ta site. There is a noticeable increase in the deviation of the Ta site in the powder sample from the centrosymmetric environment of the disordered cubic perovskite, signaled by the increased root-mean-square deviation of the two symmetry-inequivalent Ta−O bond lengths from the mean in comparison with those of the pellet sample (Tables 8 and 9). In addition, the Ta cation is displaced 0.0761(1) Å for the pellet and 0.0817(1) Å for the powder sample from the center of the oxygen octahedron, reflecting enhanced Ta−O multiple bonding characteristic of d^0 early transition metals (Figure 11). The changes in the environments of the two symmetry-inequivalent Ba sites between the powder and pellet samples are much less pronounced than those at the octahedral sites.

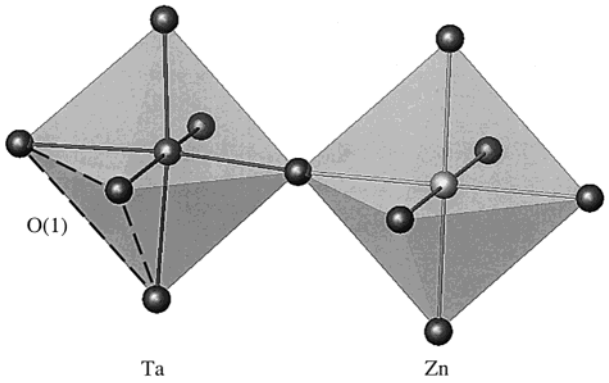

Figure 11. The Ta cation is significantly displaced away from the octahedral centroid toward the face consisting of three O(2) anions. One of the three equivalent O(1) anions making up the opposite face is indicated.

Conclusions

It is well-documented that it is demanding to achieve complete cation ordering in BZT, and this has led to considerable interest in the role of low-level B-site substitutions in enhancing the degree of ordering. Although there have been many studies of the importance of various processing parameters in controlling the structure and dielectric properties of BZT, the correlation between composition (particularly Zn loss), domain size, and the extent of cation order within the domains has not been established previously. It is not possible to quantify the extent of order based on intensities of one or two superlattice reflections due to the occurrence of Zn vacancies on the B-sites. The superstructure reflection intensities and widths depend in a complex manner on the thermal history, as the ordering is a kinetic process which is accelerated at higher temperature yet opposed thermodynamically by a decrease in the order parameter on approaching the transition temperature.[14] Here, we isolated the influence of Zn loss on the extent and homogeneity of ordering by quantitatively comparing two materials with different Zn contents prepared with identical thermal histories. The considerable differences in the phase assemblage within the two samples and the atomic-level structures of these phases indicates the extreme sensitivity of the BZT system to processing, presumably due to the difficulty in ensuring homogeneous ZnO partial pressure throughout the annealing environment. The greater ZnO loss in the powder covering the pellet is expected due to its higher surface area and lower local ZnO partial pressure. It results in larger ordered trigonal domains and an enhanced phase fraction of an ordered phase whose *c*/*a* ratio and B-site bond lengths are very similar to those in the ordered phase in the less Zn-deficient pellet sample. The heterogeneity observed between the pellet and the powder covering it is demonstrated by both analytical TEM and diffraction probes and suggests that even within each of these two distinct parts of the sample the atomic-level structure may differ, reflecting the difficulty of homogenizing both the Zn concentration and the Zn/Ta site ordering.

Detailed inspection of the diffraction data indicates that there are two distinct BZT trigonal perovskite phases within both the powder and the pellet. The distinction between the two phases is unambiguous as they have well-defined and different *c*/*a* ratios; the detailed differences emerge from the quantitative analysis of the diffraction data. These phases have different

crystalline domain extents and differ in the extent of Zn/Ta order, both being enhanced by the loss of Zn in the powder sample. In agreement with the analytical data, Zn deficiency in both samples is *required* to fit the diffraction data quantitatively, although parameter correlation in the Rietveld refinements prevents unambiguous identification of whether this deficiency lies in the more or less ordered phase. The refinements indicate, via the cell volume comparison between the two BZT phases in each sample, that the well-ordered phases in both cases are not the Zn-deficient ones, suggesting a complex ordering mechanism in which a Zn-deficient less-ordered phase assists the growth of well-ordered domains in a second phase which is microscopically almost identical in both pellet and powder samples. As both phases within each sample are ordered (as they are trigonal rather than cubic) and differ only in the details of their unit cell level structure, this type of heterogeneity is hard to identify in TEM measurements. The presence of the highly Zn-deficient impurity phase together with the more highly ordered and larger domain BZT phases in the powder sample is consistent with the importance of Zn loss in driving cation ordering in pure BZT. The BZT structure is only capable of tolerating a low level of Zn B-site vacancies before a related structure with face- as well as corner-sharing octahedra is stabilized—these octahedral vacancies may be sufficiently mobile to enhance the cation diffusion processes responsible for ordering within trigonal BZT, leading to both enhanced trigonal domain sizes and greater Zn/Ta differentiation within the domains. This is particularly important for BZT with a high order−disorder transition temperature. The coexistence of two trigonal phases as the spatial extent of coherent ordering increases indicates at least partial cation order in both and requires modification of simple nucleation and growth models to understand the evolution of cation-ordered domains in BZT.

Acknowledgment. We are grateful to the UK EPSRC for funding under GR/M62433 and access to ISIS and the SRS. We thank Dr. David Iddles (Filtronic Comtek plc) for his enthusiastic support of this work and many useful discussions.

CM020461E